# Cage-Type Hexanuclear Platinum(0) Clusters with Diphosphine and Isocyanide Ligands Encapsulating Two Mercury(0) Atoms

Tomoaki Tanase,*,† Eri Goto,† Hiroe Takenaka,† Takashi Horiuchi,‡ Yasuhiro Yamamoto,‡ Junpei Kuwabara,§ and Kohtaro Osakada§

*Department of Chemistry, Faculty of Science, Nara Women's University, Kitauoya-higashi-machi, Nara 630-8285, Japan, Department of Chemistry, Faculty of Science, Toho University, 2-2-1 Miyama, Funabashi, Chiba 274-8510, Japan, and Chemical Resources Laboratory, Tokyo Institute of Technology, 4259 Nagatsuda, Midori-ku, Yokohama 226-8503, Japan*

*Received September 28, 2004*

Reduction of a mixture containing $[PtCl_2(cod)]$, aromatic isocyanide (RNC; R = 2,6-xylyl (Xyl), 2,4,6-mesityl (Mes)), diphosphine ($Ph_2P(CH_2)_nPPh_2$; $n$ = 5 (dpppn), $n$ = 6 (dpphx)), and $NH_4PF_6$ by sodium amalgam (<1%) afforded trigonal-antiprismatic hexanuclear platinum(0) clusters encapsulating two mercury(0) atoms, $[Hg_2Pt_6(\mu\text{-RNC})_6(\mu\text{-diphos})_3]$ (diphos = dpphx, R = Xyl (**6a**); diphos = dpppn, R = Xyl (**8a**), Mes (**8b**)). Complexes **6a** and **8a** were characterized by X-ray crystallographic analyses to demonstrate that two triangular platinum(0) units, $\{Pt_3(\mu\text{-RNC})_3\}$, are connected by three diphosphine ligands with long methylene chains to form a closed cage of the cluster-based metallocryptand, in which two mercury(0) atoms are incarcerated with a notably short Hg−Hg distance. In complex **8a** ($n$ = 5), the centroids of the two Pt(0) triangles are linearly arranged with respect to the Hg−Hg axis to form a pseudo-$D_3$-symmetrical $Hg_2Pt_6$ antiprismatic cluster core (average Pt−Pt = 2.6719 Å, average Pt−Hg = 2.9417 Å, and Hg−Hg = 2.8424(2) Å). In contrast, in complex **6a** ($n$ = 6) the two triplatinum planes glide away from the dimercury axis to lose the $D_3$ symmetry (average Pt−Pt = 2.639 Å, average Pt−Hg = 2.923 Å, and Hg−Hg = 2.826(2) Å). The electronic structures of the $Pt_3Hg_2Pt_3$ cluster frameworks are discussed on the basis of molecular orbital calculations with EHMO and DFT methods. $Hg_2Pt_6$ clusters with an incomplete open-cage structure, $[Hg_2Pt_6(\mu\text{-RNC})_6(RNC)_2(\mu\text{-diphos})_2]$ (diphos = dpphx, R = Xyl (**7a**); diphos = dpppn, R = Mes (**9b**)), were also isolated as minor products and were transformed into the closed-cage clusters **6a** and **8b** by treatment with an equivalent diphosphine ligand. By using dppb ($n$ = 4), an open-cage mixed-metal cluster with a single mercury atom, $[HgPt_6(\mu\text{-RNC})_6(RNC)_2(\mu\text{-dppb})_2]$ (R = Xyl (**10a**), Mes (**10b**)), was obtained as the sole product. When the aliphatic isocyanide *t*-BuNC was used in the reduction with dpphx, the $Hg_2Pt_6$ mixed-metal cluster was not produced, and instead, the PtHgPt trinuclear complex $[HgPt_2(\mu\text{-dpphx})_3]$ (**11**) was obtained in a low yield and was characterized by X-ray crystallography to demonstrate the linear trinuclear structure with a considerable attractive Pt−Hg interaction (average Pt−Hg = 2.7930 Å and Pt−Hg−Pt = 179.591(3)°). The electronic structures of **11** are also discussed.

## Introduction

Transition-metal clusters with high nuclearity have intrinsic importance in constructing nanostructured metal-based molecular devices and metal-surface mimetic catalytic systems.[1] Assembling small-size clusters as building blocks is regarded as one of the strategic synthetic methodologies to build up such clusters, and in this context, the well-studied triangular triplatinum(0) complexes are versatile precursors for homo- and heterometallic clusters with higher nuclearity.[2] Triplatinum units with carbonyl ligands, $[Pt_3(\mu\text{-CO})_3(CO)_3]$, are stacked under reductive conditions to the form trigonal-prismatic clusters $[Pt_3(\mu\text{-CO})_3(CO)_3]_n^{2-}$ ($n$ = 1−10), which are known from the pioneering work by Chini.[3] Triplatinum complexes with terminal phosphines, $[Pt_3(\mu\text{-CO})_3(PR_3)_{3-4}]$, formally act as Lewis bases and react with Lewis acidic metal fragments, ML (M = Cu(I), Ag(I), Au(I); L = phosphine, halide), $MX_2$ (M =

* To whom correspondence should be addressed. E-mail: tanase@cc.nara-wu.ac.jp.
† Nara Women's University.
‡ Toho University.
§ Tokyo Institute of Technology.

(1) (a) Fackler, J. P., Ed. *Metal−Metal Bonds and Clusters in Chemistry and Catalysis*; Plenum: New York, 1990. (b) Adams, D. A., Cotton, F. A., Eds. *Catalysis by Di- and Polynuclear Metal Cluster Complexes*; Wiley-VCH: New York, 1998.

(2) (a) Imhof, D.; Venanzi, L. M. *Chem. Soc. Rev.* **1994**, 185. (b) Cross. R. J. In *Comprehensive Organometallic Chemistry*, 2nd ed.; Pergamon: Oxford, U.K., 1995; Vol. 9, Chapter 7. (c) Burrows, A. D.; Mingos, D. M. P. *Coord. Chem. Rev.* **1996**, *154*, 19. (d) Puddephatt, R. J.; Manojlovic-Muir, K. W. *Polyhedron* **1990**, *9*, 2767.

(3) (a) Longoni, P.; Chini, P. *J. Am. Chem. Soc.* **1976**, *98*, 7225. (b) Chini, P. *J. Organomet. Chem.* **1980**, *200*, 37.

10.1021/om049251x CCC: $30.25 
Publication on Web 12/21/2004

**Chart 1**

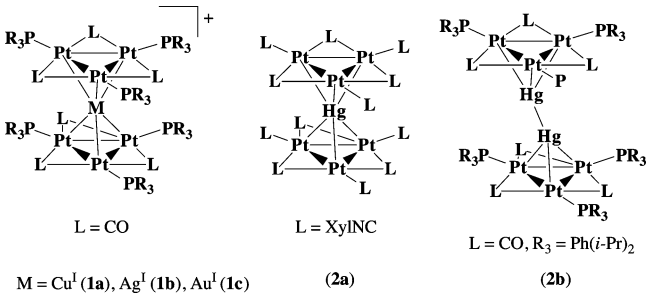


**Chart 2**

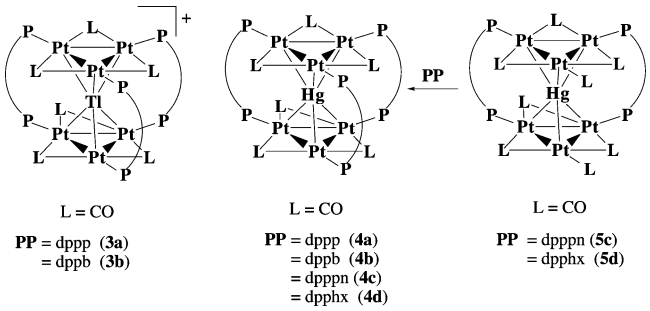


Zn(II), Cd(II); X = Br, I), and $InBr_3$, to afford heterometallic tetranuclear clusters with the M unit capping the triplatinum face.[4] The bicapped pentanuclear clusters have also been synthesized; characterized examples are $[\{Pt_3(\mu\text{-}CO)_3(PR_3)_3\}(HgX)_2]$, $[\{Pt_3(\mu\text{-}SO)_2(\mu\text{-}Cl)(PR_3)_3\}(Au(PR_3))_2]$, and $[\{Pt_3(\mu\text{-dppm})_3\}(Au(PR_3))_2]$ (dppm = bis(diphenylphosphino)methane).[5] On the other hand, two triplatinum units of $[Pt_3(\mu\text{-}CO)_3(PR_3)_3]$ have the ability to sandwich a closed-shell $d^{10}$ metal ion, resulting in the formation of $[M\{Pt_3(\mu\text{-}CO)_3(PR_3)_3\}_2]^+$ (M = Cu(I) (**1a**), Ag(I) (**1b**), Au(I) (**1c**)) (Chart 1).[6]

The electron-deficient triplatinum units $[Pt_3(\mu\text{-dppm})_3(\mu_3\text{-}CO)]^{2+}$ (42e) and $[Pt_3(\mu\text{-dppm})_3]^{2+}$ (40e) are good electron acceptors and react with Hg(0) and Tl(I) having the $d^{10}s^2$ configuration to afford $[Hg\{Pt_3(\mu\text{-dppm})_3(\mu_3\text{-}CO)\}]^{2+}$,[7a] $[Hg_2\{Pt_3(\mu\text{-dppm})_3\}]^{2+}$,[7a] $[\{HgRuCp(CO)_2\}_2\{Pt_3(\mu\text{-dppm})_3\}]^{2+}$,[7b] $[\{Hg(ReO_4)\}_2\{Pt_3(\mu\text{-dppm})_3\}]^{2+}$,[7c] and $[Tl(L)(diketonate)\{Pt_3(\mu\text{-dppm})_3(\mu_3\text{-}CO)\}]^{n+}$ (L = $H_2O$ ($n$ = 2), $CF_3COO$ ($n$ = 1)).[7d] The 42e triplatinum(0) complexes $[Pt_3(\mu\text{-}CO)_3(PR_3)_3]$ and $[Pt_3(\mu\text{-}CNR)_3(CNR)_3]$ (R = Xyl) are also able to potentially act as electron-acceptor units bound to Hg(0) and Tl(I); however, the structurally characterized examples are strictly limited to the sandwich clusters $[Hg\{Pt_3(\mu\text{-}CNR)_3(CNR)_3\}_2]$ (**2a**, R = Xyl)[8] and $[Hg_2\{Pt_3(\mu\text{-}CO)_3(PPh(i\text{-}Pr)_2)_3\}_2]$ (**2b**)[9] (Chart 1) as well as the monocapped tetranuclear cluster $[Tl\{Pt_3(\mu\text{-}CO)_3(PCy_3)_3\}]^+$.[10] In the cluster **2b**, two zerovalent mercury atoms are incorporated between the two triangles with a remarkably weak Hg−Hg interaction (3.225(1) Å). Puddephatt et al. have reported the cage-type clusters by using diphosphine ligands ($Ph_2P(CH_2)_nPPh_2$), where two $\{Pt_3(\mu\text{-}CO)_3\}$ triangular fragments are connected by three diphosphines and a Tl(I) ion or a Hg(0) atom is encapsulated in the cage (Chart 2).[11] Three synthetic routes to the mixed-metal cage clusters $[TlPt_6(\mu\text{-}CO)_6(\mu\text{-}Ph_2P(CH_2)_nPPh_2)_3]^+$ (**3**: $n$ = 3, 4) and $[HgPt_6(\mu\text{-}CO)_6(\mu\text{-}Ph_2P(CH_2)_nPPh_2)_3]$ (**4**: $n$ = 3−6) were established. (i) The open-type hexaplatinum(0) cluster $[Pt_6(\mu\text{-}CO)_6(\mu\text{-dppp})_2(dppp)_2]$ reacted with Hg(0) or Tl(I) to afford the cluster **3a** or **4a** by the loss of one dppp ligand (dppp = 1,3-bis(diphenylphosphino)propane ($n$ = 3)). (ii) With 1,4-bis(diphenylphosphino)butane (dppb, $n$ = 4), reduction of $[PtCl_2(SMe_2)_2]$ by $NaBH_4$, in the presence of CO, dppb, and Hg(0) or Tl(I), yielded the cluster **3b** or **4b**. (iii) By a similar reduction with the longer chain diphosphines (1,5-bis(diphenylphosphino)pentane (dpppn, $n$ = 5) and 1,6-bis(diphenylphosphino)hexane (dpphx, $n$ = 6)), the open-type cage clusters of $[HgPt_6(\mu\text{-}CO)_6(CO)_2(\mu\text{-diphos})_2]$ (**5c**,**d**) and the closed-type clusters of $[HgPt_6(\mu\text{-}CO)_6(diphos)_3]$ (**4c**,**d**) were obtained (diphos = dpppn, dpphx); the open-type clusters **5c**,**d** were readily converted into the closed clusters **4c**,**d** by treatment with 1 equiv of the diphosphines. Among these clusters, compound **3a** was characterized by X-ray crystallography to demonstrate that the three-methylene chain of dppp is just accommodated to incarcerate a single metal between the two $Pt_3$ triangles. Interestingly, only one mercury atom was incorporated, even with the diphosphines having longer methylene chains, dpppn ($n$ = 5) and dpphx ($n$ = 6), despite the fact that two triplatinum(0) units with monodentate phosphine ligands sandwich two mercury atoms, as shown in **2b**.[9]

During our studies to explore systematic synthetic routes to di-, tri-, and multinuclear platinum and palladium complexes by utilizing diphosphine supporting ligands,[12] it was found that reduction of $[PtCl_2(cod)]$ by sodium amalgam in the presence of bulky aromatic isocyanides and diphosphines with long methylene chains (dpppn, dpphx) gave rise to the cage-type clusters, where two triangular $Pt_3$ units are held together

(4) (a) Stockhammer, A.; Dahmen, K.-H.; Gerfin, T.; Gramlich, V.; Peter, W.; Venanzi, L. M. *Helv. Chim. Acta* **1991**, *74*, 989. (b) Imhof, D.; Burckhardt, U.; Dahmen, K.-H.; Rüegger, H.; Gerfin, T.; Gramlich, V. *Inorg. Chem.* **1993**, *32*, 5206. (c) Mingos, D. M. P.; Wardle, R. W. M. *J. Chem. Soc., Dalton Trans.* **1986**, 73. (d) Hill, C. M.; Mingos, D. M. P.; Powell, H.; Watson, M. J. *J. Organomet. Chem.* **1992**, *441*, 499. (e) Briant, C. E.; Wardle, R. W. M.; Mingos, D. M. P. *J. Organomet. Chem.* **1984**, *267*, C49. (f) Imhof, D.; Burchhardt, U.; Dahmen, K.-H.; Joho, F.; Nesper, R. *Inorg. Chem.* **1997**, *36*, 1813. (g) Bhaduri, S.; Sharma, K.; Jones, P. G.; Erdbrugger, C. F. *J. Organomet. Chem.* **1987**, *326*, C46. (h) Bour, J. J.; Kanters, R. P. F.; Schlebos, P. P. J.; Bos, W.; Bosman, W. P.; Behm, H.; Beurskens, P. T.; Steggerda, J. J. *J. Organomet. Chem.* **1987**, *329*, 405. (i) Burrows, A. D.; Jeffrey, J. G.; Machell, J. C.; Mingos, D. M. P. *J. Organomet. Chem.* **1991**, *406*, 399. (j) Braunstein, P.; Freyburger, S.; Bars, O. *J. Organomet. Chem.* **1988**, *352*, C29.

(5) (a) Albinati, A.; Dahmen, K.-H.; Demartin, F.; Forward, J. M.; Longley, C. J.; Mingos, D. M. P.; Venanzi, L. M. *Inorg. Chem.* **1992**, *31*, 2223. (b) Mingos, D. M. P.; Oster, P.; Sherman, D. J. *J. Organomet. Chem.* **1987**, *320*, 257. (c) Payne, N. C.; Ramachandran, R.; Schoettel, R.; Vittal, J. J.; Puddephatt, R. J. *Inorg. Chem.* **1991**, *30*, 4048.

(6) (a) Albinati, A.; Dahmen, K.-H.; Togni, A.; Venanzi, L. M. *Angew. Chem., Int. Ed. Engl.* **1985**, *24*, 766. (b) Hallam, M. F.; Mingos, D. M. P.; Adatia, T.; McPartin, M. *J. Chem. Soc., Dalton Trans.* **1988**, 335.

(7) (a) Schoettel, G.; Vittal, J. J.; Puddephatt, R. J. *J. Am. Chem. Soc.* **1990**, *112*, 6400. (b) King, W. D.; Lukehart, C. M. *J. Cluster Sci.* **1998**, *9*, 107. (c) Hao, L.-J.; Xiao, J.-L.; Vittal, J. J.; Puddephatt, R. J.; Manojlovic-Muir, L.; Muir, K. W.; Torabi, A. A. *Inorg. Chem.* **1996**, *35*, 658. (d) Stadnichenko, R.; Sterenberg, B. T.; Bradford, A. M.; Jennings, M. C.; Puddephatt, R. J. *J. Chem. Soc., Dalton Trans.* **2002**, 1212.

(8) (a) Yamamoto, Y.; Yamazaki, H.; Sakurai, T. *J. Am. Chem. Soc.* **1982**, *104*, 2329. (b) Yamamoto, Y.; Yamazaki, H. *Inorg. Chim. Acta* **1994**, *217*, 121.

(9) Albinati, A.; Moor, A.; Pregosin, P. S.; Venanzi, L. M. *J. Am. Chem. Soc.* **1982**, *104*, 7672.

(10) Ezomo, O. J.; Mingos, D. M. P.; Williams, I. D. *J. Chem. Soc., Chem. Commun.* **1987**, 924.

(11) (a) Hao, L.; Vittal, J. J.; Puddephatt, R. J. *Inorg. Chem.* **1996**, *35*, 269. (b) Hao, L.; Vittal, J. J.; Puddephatt, R. J. *Organometallics* **1996**, *15*, 3115.

(12) (a) Tanase, T.; Yamamoto, Y.; Puddephatt, R. J. *Organometallics* **1996**, *15*, 1502. (b) Tanase, T.; Ukaji, H.; Kudo, Y.; Ohno, M.; Kobayashi, K.; Yamamoto, Y. *Organometallics* **1994**, *13*, 1374.

by the diphosphine ligands and two mercury atoms are encapsulated in the cage. We wish to report herein the full details of the synthesis and characterization for the $Hg_2Pt_6$ mixed-metal clusters with diphosphines. A preliminary account of this work has already been reported.[13]

## Experimental Section

All manipulations were carried out under a nitrogen atmosphere with standard Schlenk techniques. Reagent grade solvents were dried by the standard procedures and were freshly distilled prior to use. IR spectra were recorded on a Jasco FT/IR-410 spectrophotometer, and electronic absorption spectra were acquired on Shimadzu UV-3100 and Hewlett-Packard Agilent 8453 spectrophotometers. $^1$H and $^{31}$P{$^1$H} NMR spectra were recorded on a Varian Gemini 2000 spectrometer at 300 and 121 MHz, respectively. $^1$H NMR spectra were referenced to TMS as external standard, and $^{31}$P{$^1$H} NMR spectra were referenced to 85% $H_3PO_4$ as external standard. ESI-TOF mass spectra were recorded on an Applied Biosystems Mariner high-resolution mass spectrometer with positive ionization mode. The following abbreviations are used: 1,6-bis(diphenylphosphino)hexane (dpphx), 1,5-bis(diphenylphosphino)pentane (dpppn), 1,4-bis(diphenylphosphino)butane (dppb), 1,3-bis(diphenylphosphino)propane (dppp), 1,2-bis(diphenylphosphino)ethane (dppe), and bis(diphenylphosphino)methane (dppm).

**Preparation of [$Hg_2Pt_6$($\mu$-RNC)$_6$($\mu$-dpphx)$_3$] (R = Xyl (6a)) and [$Hg_2Pt_6$($\mu$-RNC)$_6$(RNC)$_2$($\mu$-dpphx)$_2$] (R = Xyl (7a)).** A mixture of [$PtCl_2$(cod)] (100 mg, 0.27 mmol), XylNC (71 mg, 0.54 mmol), dpphx (123 mg, 0.27 mmol), and $NH_4PF_6$ (88 mg, 0.54 mmol) in THF (30 mL) was treated with sodium amalgam (<1%) for several hours at room temperature. The color of the solution changed from pale yellow to dark green, and the solution was passed through a short alumina column (10 wt % deactivated). The solution was concentrated to dryness, and the residue was crystallized from a benzene/hexane mixed solvent at 2 °C to give dark green rectangular crystals of [$Hg_2Pt_6$($\mu$-XylNC)$_6$($\mu$-dpphx)$_3$]·$C_6H_6$ (**6a**·$C_6H_6$) in 38% yield, which were collected by filtration, washed with hexane, and dried under vacuum. From the mother liquor, a green powder of [$Hg_2Pt_6$($\mu$-XylNC)$_6$(XylNC)$_2$($\mu$-dpphx)$_2$]·$C_6H_6$ (**7a**·$C_6H_6$) was obtained in 5% yield. Data for **6a**·$C_6H_6$ are as follows. Anal. Calcd for $C_{150}H_{156}N_6P_6Hg_2Pt_6$: C, 47.41; H, 4.14; N, 2.21. Found: C, 47.34; H, 4.16; N, 2.14. IR (Nujol, cm$^{-1}$): 1834 m, 1711 (N=C). UV−vis (in benzene; nm (log $\epsilon$)): 642 (3.91), 437 (3.75), 332 (3.93). $^1$H NMR (300 MHz, room temperature, in THF-$d_8$): $\delta$ 2.48 (s, 36H, *o*-Me), 6.2−7.8 (m, 78H, Ar). $^{31}$P{$^1$H} NMR (121 MHz, room temperature, in THF-$d_8$): $\delta$ 44.1 (s, 6P, $^1J_{PtP}$ = 4904, $^2J_{PtP}$ = 451 Hz). ESI-MS (in THF): *m/z* 3722.917 (*z*1, {[$Hg_2Pt_6$($\mu$-XylNC)$_6$(dpphx)$_3$] + H}$^+$ (3722.772)). Data for **7a**·$C_6H_6$ are as follows. Anal. Calcd for $C_{138}H_{142}N_8P_4Hg_2Pt_6$: C, 45.94; H, 3.97; N, 3.11. Found: C, 46.46; H, 4.10; N, 3.10. IR (Nujol, cm$^{-1}$): 2104, 1901 (N≡C), 1690, 1661 (N=C). UV−vis (in benzene; nm (log $\epsilon$)): 670 (3.55), 463 (3.47), 327 (3.67). The NMR spectrum of **7a** was not measured, due to very low solubility.

**Preparation of [$Hg_2Pt_6$($\mu$-RNC)$_6$($\mu$-dpppn)$_3$] (R = Xyl (8a), Mes (8b)) and [$Hg_2Pt_6$($\mu$-RNC)$_6$(RNC)$_2$($\mu$-dpppn)$_2$] (R = Mes (9b)).** By a procedure similar to that mentioned above, with dpppn and MesNC, the clusters [$Hg_2Pt_6$($\mu$-MesNC)$_6$($\mu$-dpppn)$_3$]·$C_6H_6$ (**8b**) and [$Hg_2Pt_6$($\mu$-MesNC)$_6$(MesNC)$_2$($\mu$-dpppn)$_2$]·$C_6H_6$ (**9b**) were obtained in 10% and 7% yields, respectively. Data for **8b**·$C_6H_6$ are as follows. Anal. Calcd for $C_{153}H_{162}N_6P_6Hg_2Pt_6$: C, 47.83; H, 4.25; N, 2.19. Found: C, 47.65; H, 4.10; N, 2.18. IR (Nujol, cm$^{-1}$): 1857 m, 1714 (N=C). UV−vis (in benzene; nm (log $\epsilon$)): 662 (3.97), 430 (3.67), 325 (3.86). ESI-MS (in THF): *m/z* 3765.956 (*z*1, {[$Hg_2Pt_6$($\mu$-MesNC)$_6$(dpppn)$_3$] + H}$^+$ (3765.827)). Data for **9b**·$C_6H_6$ are as follows. Anal. Calcd for $C_{144}H_{154}N_8P_4Hg_2Pt_6$: C, 46.84; H, 4.20; N, 3.03. Found: C, 46.98; H, 4.17; N, 2.95. IR (Nujol, cm$^{-1}$): 2110, 1933 (N≡C), 1700, 1662 (N=C). UV−vis (in benzene; nm (log $\epsilon$)): 676 (3.85), 466 (3.77), 346 (3.97). By a similar procedure with XylNC, the closed-type cluster [$Hg_2Pt_6$($\mu$-XylNC)$_6$($\mu$-dpppn)$_3$]·$C_6H_6$ (**8a**·$C_6H_6$) was obtained in crystalline form in 18% yield, although the open-type cluster was not isolated in the pure form. Data for **8a**·$C_6H_6$ are as follows. Anal. Calcd for $C_{147}H_{150}N_6P_6Hg_2Pt_6$: C, 46.98; H, 4.02; N, 2.24. Found: C, 46.74; H, 3.90; N, 2.29. IR (Nujol, cm$^{-1}$): 1851 m, 1671 (N=C). UV−vis (in benzene; nm (log $\epsilon$)): 662 (4.21), 406 (3.94). ESI-MS (in THF): *m/z* 3680.725 (*z*1, {[$Hg_2Pt_6$($\mu$-XylNC)$_6$(dpppn)$_3$] + H}$^+$ (3681.119)). The NMR spectra of **8a**,**b** and **9b** were not measured, owing to low solubility.

**Preparation of [$HgPt_6$($\mu$-RNC)$_6$(RNC)$_2$($\mu$-dppb)$_2$] (R = Xyl (10a), Mes (10b)).** A mixture of [$PtCl_2$(cod)] (100 mg, 0.27 mmol), XylNC (71 mg, 0.54 mmol) or MesNC (78 mg, 0.54 mmol), dppb (115 mg, 0.27 mmol), and $NH_4PF_6$ (88 mg, 0.54 mmol) in benzene (30 mL) was treated with sodium amalgam (<1%) for several hours at room temperature. The color of the solution changed from pale yellow to dark green, and the solution was passed through a short alumina column (10 wt % deactivated). The solution was concentrated to dryness, and the residue was crystallized from a benzene/hexane mixed solvent at 2 °C to afford dark green powders of [$HgPt_6$($\mu$-RNC)$_6$(RNC)$_2$($\mu$-dppb)$_2$]·$C_6H_6$ (R = Xyl (**10a**), 62%; R = Mes (**10b**), 52%). Data for **10a**·$C_6H_6$ are as follows. Anal. Calcd for $C_{134}H_{134}N_8P_4HgPt_6$: C, 48.02; H, 4.03; N, 3.34. Found: C, 47.70; H, 4.32; N, 2.87. IR (Nujol, cm$^{-1}$): 2088, 1897 (C≡N), 1741, 1660 (N=C). UV−vis (in benzene; nm (log $\epsilon$)): 651 (3.57), 445 (3.40), 356 (3.65). ESI-MS (in THF): *m/z* 3273.627 (*z*1, {[$HgPt_6$(XylNC)$_8$(dppb)$_2$] + H}$^+$ (3273.688)). Data for **10b**·$C_6H_6$ are as follows. Anal. Calcd for $C_{142}H_{150}N_8P_4HgPt_6$: C, 49.24; H, 4.36; N, 3.24. Found: C, 48.87; H, 4.39; N, 3.37. IR (Nujol, cm$^{-1}$): 2067, 1860 (N≡C), 1800, 1664 (N=C). UV−vis (in benzene; nm (log $\epsilon$)): 643 (3.74), 460 (3.40), 340 (3.92). ESI-MS (in THF): *m/z* 3286.119 (*z*1, {[$HgPt_6$(MesNC)$_8$(dppb)$_2$] + H}$^+$ (3285.820)). The NMR spectra of **10a**,**b** were not measured, owing to low solubility.

**Preparation of [$HgPt_2$(dpphx)$_3$]·3.5$C_6H_6$ (11·3.5$C_6H_6$).** A procedure similar to that described in the preparation of **6a**, but using *t*-BuNC, gave a bright red solution. The solution was concentrated to dryness, and the residue was extracted with benzene. The extract was concentrated to afford dark green/red dichroic crystals of [$HgPt_2$(dpphx)$_3$]·3.5$C_6H_6$ (**11**·3.5$C_6H_6$) in 7% yield, which were characterized by spectroscopic techniques and an X-ray crystallographic analysis. IR (KBr, cm$^{-1}$): 1670 br, 1435 s, 1178, 1088, 735 s, 694 s, 508. UV−vis (in benzene; nm (log $\epsilon$)): 502 (4.61), 317 (4.35), 287 (4.18). $^{31}$P{$^1$H} NMR (121 MHz, room temperature, THF-$d_8$): $\delta$ 22.1 (s, 6P, $^1J_{PtP}$ = 4453 Hz). ESI-MS (in THF): *m/z* 1955.623 (*z*1, {[$HgPt_2$(dpphx)$_3$] + H}$^+$ (1955.503)).

**X-ray Crystallographic Analyses of 6a, 8a·$CH_3(CH_2)_4CH_3$, and 11·3.5$C_6H_6$.** The large block-shaped crystals of **6a**, **8a**·$CH_3(CH_2)_4CH_3$, and **11**·3.5$C_6H_6$, suitable for X-ray crystallography, were obtained by slow recrystallization from a benzene/hexane mixed solvent at low temperature and were fixed on top of a glass fiber with Paratone N oil. Crystal data and experimental conditions are summarized in Table 1. Reflection data for **6a** were remeasured with a CCD diffractometer to improve the quality of X-ray crystallographic analysis.[13] All data were collected at −120 °C on a Rigaku AFC8R/Mercury CCD diffractometer equipped with graphite-monochromated Mo K$\alpha$ radiation using a rotating-anode X-ray generator. A total of 2160 oscillation images, covering the whole sphere of $2\theta < 55°$, were collected with exposure rates of 120° s$^{-1}$ (**8a**) and 128° s$^{-1}$ (**11**) by the $\omega$-scan method ($-62 < \omega < 118°$) with $\Delta\omega = 0.25°$, and 1440 images covering the sphere of $2\theta < 52°$ were collected for **6a** with exposure rates

(13) Tanase, T.; Horiuchi, T.; Yamamoto, Y.; Kobayashi, K. *J. Organomet. Chem.* **1992**, *440*, 1.

**Table 1. Crystallographic and Experimental Data for $[Hg_2Pt_6(\mu\text{-XylNC})_6(\mu\text{-dpphx})_3]$ (6a), $[Hg_2Pt_6(\mu\text{-XylNC})_6(\mu\text{-dpppn})_3]\cdot C_6H_{14}$ (8a), and $[HgPt_2(\mu\text{-dpphx})_3]\cdot 3.5C_6H_6$ (11·3.5C$_6$H$_6$)**

| | **6a** | **8a**·C$_6$H$_{14}$ | **11**·3.5C$_6$H$_6$ |
|---|---|---|---|
| formula | $C_{144}H_{150}N_6P_6Pt_6Hg_2$ | $C_{147}H_{158}N_6P_6Pt_6Hg_2$ | $C_{111}H_{117}P_6Pt_2Hg$ |
| fw | 3722.37 | 3766.47 | 2227.76 |
| cryst syst | monoclinic | monoclinic | triclinic |
| space group | *C*2/*c* (No. 15) | *P*2/*n* (No. 13) | $P\bar{1}$ (No. 2) |
| *a*, Å | 38.202(4) | 16.571(2) | 14.8858(8) |
| *b*, Å | 14.8735(11) | 15.024(2) | 15.2745(7) |
| *c*, Å | 30.618(3) | 21.980(2) | 23.2773(9) |
| α, deg | 90 | 90 | 93.889(1) |
| *β*, deg | 115.632(1) | 96.519(6) | 101.819(2) |
| *γ*, deg | 90 | 90 | 111.113(2) |
| *V*, Å$^3$ | 15685(3) | 8431(1) | 4774.2(4) |
| *Z* | 4 | 2 | 2 |
| *T*, °C | -120 | -120 | -120 |
| $D_{calcd}$, g cm$^{-3}$ | 1.576 | 1.483 | 1.550 |
| abs coeff, cm$^{-1}$ | 73.67 | 68.54 | 46.68 |
| 2*θ* range, deg | $6 < 2\theta < 50$ | $6 < 2\theta < 55$ | $6 < 2\theta < 55$ |
| no. of unique data | 6775 | 19 860 | 13 523 |
| no. of obsd data | 3688 ($I > 3\sigma(I)$) | 12 879 ($I > 2\sigma(I)$) | 12 555 ($I > 2\sigma(I)$) |
| no. of variables | 418 | 739 | 1082 |
| data/param ratio | 8.82 | 17.43 | 11.60 |
| $R^a$ | 0.084 | 0.079 | 0.033 |
| $R_w$ or wR2 | 0.089[b] | 0.243[c] | 0.066[d] |

[a] $R = \sum||F_o| - |F_c||/\sum|F_o|$. [b] $R_w = [\sum w(|F_o| - |F_c|)^2/\sum w|F_o|^2]^{1/2}$ ($w = 1/\sigma^2(F_o)$). [c] $wR2 = [\sum w(F_o^2 - F_c^2)^2/\sum w(F_o)^2]^{1/2}$ (for all data, $w = 1/[\sigma^2(F_o) + (0.1178P)^2 + 111.2125P]$, $P = (F_o^2 + 2F_c^2)/3$). [d] $wR2 = [\sum w(F_o^2 - F_c^2)^2/\sum w(F_o^2)^2]^{1/2}$ ($w = 1/\sigma^2(F_o^2)$).

of 128° s$^{-1}$ by the *ω*-scan method ($-70 < \omega < 110°$) with $\Delta\omega = 0.25°$. The crystal-to-detector (70 × 70 mm) distance was set to 60 mm. The data were processed using the program Crystal Clear 1.3.5 (Rigaku/MSC)[14] and corrected for Lorentz–polarization and absorption effects. The structure of **6a** was solved by direct methods (SIR97)[15] and refined on *F* with full-matrix least-squares techniques with teXsan.[16] The Hg, Pt, and P atoms were refined anisotropically, and other non-hydrogen atoms were refined with isotropic temperature factors. All hydrogen atoms were calculated and fixed in the refinement. The structures of **8a** and **11** were solved by heavy-atom methods (DIRDIF94 Patty)[17] and refined on $F^2$ by least-squares techniques with SHELXL-97 (**8a**)[18] and teXsan (**11**). All non-hydrogen atoms were refined with anisotropic thermal parameters, and the C–H hydrogen atoms were placed at calculated positions and were fixed in the refinement. The C atoms of the solvated hexane in the structure of **8a** were refined isotropically. All calculations were carried out on a Silicon Graphics O2 station with the teXsan crystallographic software package and a Pentium PC with the Crystal Structure package.[19]

**Molecular Orbital Calculations.** Single-point density functional calculations on the structures of **6a** and **8a** (determined by X-ray crystallography) were performed using the BECK3LYP method with the LANL2DZ basis set. All calculations were carried out on a Silicon Graphic Octane Station with the Gaussian 98 program package. Extended Hückel molecular orbital calculations were carried out by using parameters of the Coulomb integrals and the orbital exponents taken from the literature[20] on a Pentium PC computer. For the Hg and Pt d functions, double-*ξ* expansions were used. The fragment analyses were performed by using the program CACAO.[21]

**Chart 3**

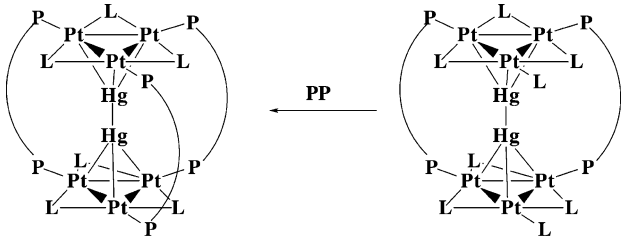


PP = dpphx, L = XylNC (**6a**)
PP = dpppn, L = XylNC (**8a**)
PP = dpppn, L = MesNC (**8b**)

PP = dpphx, L = XylNC (**7a**)
PP = dpppn, L = MesNC (**9b**)

## Results and Discussion

**Synthesis of Hexaplatinum(0) Clusters Bridged by Diphosphine Ligands Including Two Mercury Atoms.** When $[PtCl_2(cod)]$ was treated with sodium amalgam in the presence of aromatic isocyanides (RNC) and diphosphines having long methylene chains (diphos), the color of the reaction solution changed from pale yellow to dark green, from which blackish green crystals formulated as $[Hg_2Pt_6(\mu\text{-RNC})_6(\mu\text{-diphos})_3]$ were isolated (diphos = dpphx, R = Xyl (**6a**); diphos = dpppn, R = Xyl (**8a**), Mes (**8b**)) (Chart 3). The IR spectra of **6** and **8** showed very broad and intense CN stretching vibrations around 1714–1671 cm$^{-1}$, assignable to CN double bonds of bridging isocyanide ligands. In the electronic absorption spectra in benzene, a characteristic band appeared around 642 nm (**6a**) and 662 nm (**8**). The ESI mass spectra of **6a** and **8a** in THF exhibited the parent monocation peaks corresponding to $\{[Hg_2Pt_6(\mu\text{-XylNC})_6(diphos)_3]+H\}^+$ at *m/z* 3722.92 (**6a**) and *m/z* 3680.73 (**8a**), respectively. The $^1$H and $^{31}$P{$^1$H} NMR spectra of **6a** were barely measured, owing to low solubility, to show a symmetrical structure with a singlet peak for *o*-methyl protons of isocyanides and a resonance for the P atoms of dpphx ligands ($\delta$ 44.1, $^1J_{PtP} = 4904$ Hz). The detailed structures of **6a** and **8a** were determined by X-ray crystallography (vide infra) to involve a closed-cage $Hg_2Pt_6$ framework. Complexes **6** and **8** were stable under a nitrogen atmosphere even with heating in benzene, which was notably contrasted with the fact that complexes **2a**,**b** readily underwent fragmentation via dissociation of the mercury atom at higher temperature.

In the preparation of **6a** and **8b**, microcrystals of another cluster, $[Hg_2Pt_6(\mu\text{-RNC})_6(RNC)_2(diphos)_2]$ (diphos = dpphx, R = Xyl (**7a**), diphos = dpppn, R = Mes (**9b**)), were isolated as minor products. The IR spectra indicated the presence of terminal isocyanides ($\nu_{CN}$ 2104–2110 cm$^{-1}$) as well as bridging ones ($\nu_{CN}$ 1933–1661 cm$^{-1}$). In the electronic absorption spectra of **7a** and **9b**,

(14) Crystal Clear 1.3.5: Operating Software for the CCD Detector System; Rigaku and Molecular Structure Corp., 2003.
(15) Altomare, A.; Burla, M. C.; Camalli, M.; Cascarano, M.; Giacovazzo, C.; Guagliardi, A.; Polidori, G. *J. Appl. Crystallogr.* **1994**, *27*, 435.
(16) TEXSAN: Crystal Structure Analysis Package; Molecular Structure Corp., 1999.
(17) Beurskens, P. T.; Admiraal, G.; Beurskens, G.; Bosman, W. P.; de Gelder, R.; Israel, R.; Smits, J. M. M. DIRDIF-94 Program System; Technical Report of the Crystallography Laboratory; University of Nijmegen, Nijmegen, The Netherlands, 1994.
(18) Sheldrick, G. M. SHELXL-97: Program for the Refinement of Crystal Structures; University of Göttingen, Göttingen, Germany, 1996.
(19) Crystal Structure 3.6: Crystal Structure Analysis Package; Rigaku and Molecular Structure Corp., 2003.
(20) (a) Hoffmann, R. *J. Chem. Phys.* **1963**, *39*, 1397. (b) Hoffmann, R.; Lipscomb, W. N. *J. Chem. Phys.* **1962**, *36*, 2179. (c) Hoffmann, R.; Lipscomb, W. N. *J. Chem. Phys.* **1962**, *36*, 3489. (d) Ammeter, J. H.; Burgi, H.-B.; Thibeault, J. C.; Hoffmann, R. *J. Am. Chem. Soc.* **1978**, *100*, 3686.
(21) Mealli, C.; Prosterpio, D. *J. Chem. Educ.* **1990**, 67, 399.

**Chart 4**

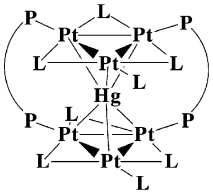

PP = dppb, L = XylNC (**10a**)
PP = dppb, L = MesNC (**10b**)

**Chart 5**

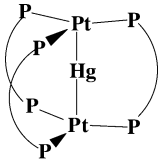

PP = dpphx (**11**)

the characteristic band shifted to lower energy around 670−676 nm, in comparison with those of the corresponding closed clusters **6a** and **8b**. By treatment with 1 equiv of the diphosphines in benzene, complexes **7a** and **9b** were readily converted into the corresponding closed-cage complexes **6a** and **8b**, respectively. From these spectral data, complexes **7a** and **9b** were estimated to have an incomplete open-cage structure as indicated in Chart 3, although the detailed structures were not elucidated.

In the cases using dpphx ($n = 6$) and dpppn ($n = 5$), single-mercury-trapped clusters, such as $[HgPt_6(\mu\text{-RNC})_6(\text{diphos})_3]$ and $[HgPt_6(\mu\text{-RNC})_6(\text{RNC})_2(\text{diphos})_2]$, were not isolated. However, a similar reaction of $[PtCl_2(\text{cod})]$ with sodium amalgam in the presence of RNC and dppb ($n = 4$) exclusively yielded the open-cage cluster in which a single mercury atom was incorporated, $[HgPt_6(\mu\text{-RNC})_6(\text{RNC})_2(\mu\text{-dppb})_2]$ (R = Xyl (**10a**), Mes (**10b**)) (Chart 4). The IR spectra for the isocyanide region were similar to those of **7a** and **9b**, and the ESI mass spectra showed the parent monovalent peaks assignable to $\{[HgPt_6(RNC)_8(\text{dppb})_2] + H\}^+$ centered at *m/z* 3273.63 (**10a**) and *m/z* 3286.12 (**10b**). Unlike complexes **7a** and **9b**, the single-mercury clusters **10a**,**b** were not converted to the closed-cage clusters of $[HgPt_6(\mu\text{-RNC})_6(\mu\text{-dppb})_3]$ by treatment with dppb. A single-mercury-trapped analogous cluster with bridging carbonyl ligands, $[HgPt_6(\mu\text{-CO})_6(\text{dppb})_3]$ (**4b**), was successfully prepared as described before; however, the isocyanide clusters **10a**,**b** slowly decomposed when treated with an excess of dppb. The steric repulsion between the phenyl groups of dppb and the bulky aromatic isocyanides may prevent the formation of the closed-cage clusters with a single mercury atom incorporated.

When *t*-BuNC was used instead of the bulky aromatic isocyanides, the reduction of $[PtCl_2(\text{cod})]$ with dpphx gave a bright red reaction solution, from which red crystals of $[HgPt_2(\mu\text{-dpphx})_3]\cdot 3.5C_6H_6$ (**11**·$3.5C_6H_6$) were isolated in low yield (Chart 5). The $\pi$-accepting ability of the bridging isocyanides is assumed to be an important factor in stabilizing the $Hg_2Pt_6$ mixed-metal clusters. The detailed structure of **11** was characterized by spectroscopic techniques and an X-ray crystallographic analysis. In the electronic absorption spectrum, a characteristic intense band was observed at 502 nm, and

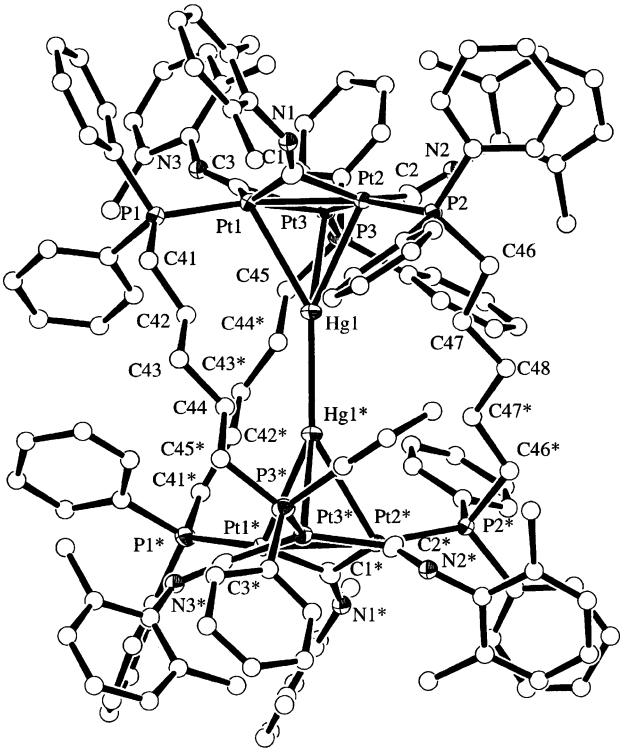


**Figure 1.** ORTEP plot of $[Hg_2Pt_6(\mu\text{-XylNC})_6(\text{dpppn})_3]$ (**8a**).

the $^{31}P\{^1H\}$ NMR spectrum exhibited a singlet peak at $\delta$ 22.1 ppm with $^{195}Pt$ satellite peaks ($^1J_{PtP} = 4453$ Hz). The $^2J_{HgP}$ coupling was not resolved. The ESI mass spectrum indicated the parent monovalent peak at *m/z* 1955.62 corresponding to $\{[HgPt_2(\text{dpphx})_3] + H\}^+$.

**Structures of $[Hg_2Pt_6(\mu\text{-XylNC})_6(\mu\text{-diphos})_3]$ (diphos = dpphx (6a), dpppn (8a)).** ORTEP plots of complex **8a** are illustrated in Figures 1 and 2, and selected bond lengths and angles are summarized in Table 2. The structure of **8a** has a crystallographically imposed $C_2$ axis passing through the C48 atom and the middle point of the Hg−Hg bond and also has a pseudo-$C_3$ axis along the Hg−Hg bond, resulting in a overall pseudo-$D_3$ symmetry. The neutral molecule is composed of two triangular triplatinum fragments, $\{Pt_3(\mu\text{-XylNC})_3\}$, connected by three dpppn ligands, forming a large closed-cage in which two mercury atoms are incorporated. In other words, two $HgPt_3$ tetrahedrons are joined by an Hg−Hg bonding interaction to construct an antiprismatic $Pt_3Hg_2Pt_3$ mixed-metal framework. The centroids of the $Pt_3$ triangles ($CenPt_3$) and the two Hg atoms are almost linearly arranged ($CenPt_3$−Hg1−Hg1* = 179.0°) (Figure 2a), and the two $Pt_3$ triangles are parallel, with a dihedral angle of 1.1° in a staggered form (Figure 2b). The centroid-to-centroid separation between the two $Pt_3$ triangles is 7.851 Å, and the average P−P separation of the dpppn ligands is 8.024 Å. The Hg1−Hg1* bond length is 2.8424(2) Å, which is remarkably shorter than that of the carbonyl cluster **2b** (3.225(1) Å).[9] The value is slightly shorter than is found in the crystalline α form of metallic Hg (2.99 Å) but is longer than those of $Hg_2X_2$ salts (X = halide, 2.49−2.69 Å).[22] From these parameters, the strength of the Hg−Hg bonding interaction of **8a** is estimated to be inter-

(22) Wells, A. F. *Structural Chemistry*, 4th ed.; Oxford University Press: London, 1975.

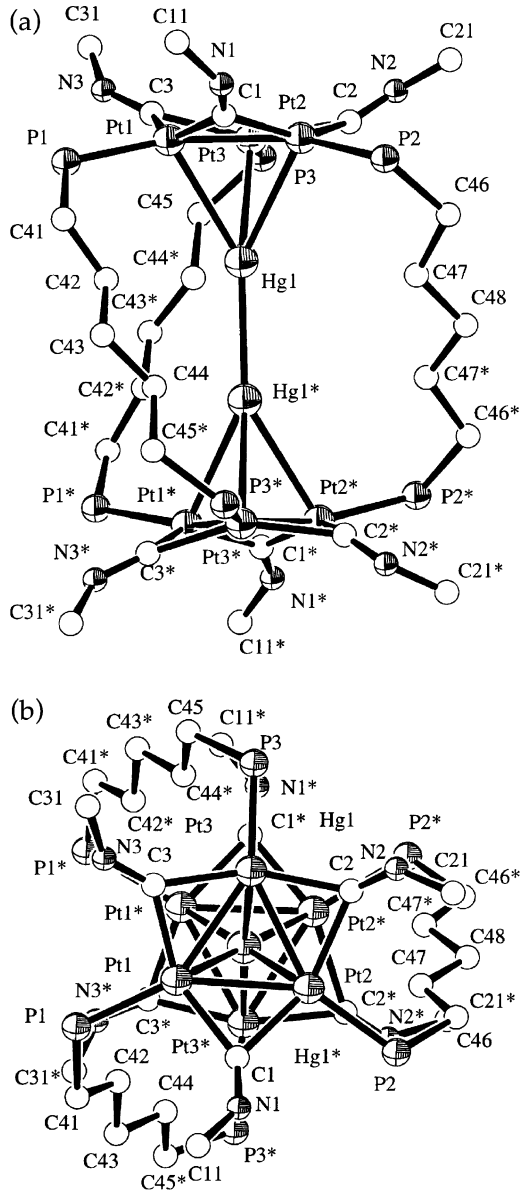


**Figure 2.** ORTEP diagrams for the cluster core of $[Hg_2Pt_6(\mu\text{-XylNC})_6(dpppn)_3]$ (**8a**) viewed (a) vertical to and (b) along the Hg−Hg axis. The phenyl and xylyl rings are omitted for clarity.

vening between Hg−Hg covalent and metallic bonds and, interestingly, is in contrast to the much weaker interaction in the carbonyl cluster **2b**. The Hg atom symmetrically caps the $Pt_3$ triangle with the bond distances of Hg1−Pt1 = 2.9448(1) Å, Hg1−Pt2 = 2.9541(1) Å, and Hg1−Pt3 = 2.9263(4) Å (average 2.945 Å), which are considerably longer than the Pt−Hg covalent bonds observed in $[(\eta^5\text{-}C_5H_5)WHgPt(PPh_3)_2(C_6Cl_5)]$ (2.572(1) Å)[23] and $[HgPt_2(\mu\text{-dppp})_2(XylNC)_2](PF_6)_2$ (average 2.640 Å)[12a] and are comparable to those found in **2a** (average 2.943 Å),[8] indicating the presence of a weak bonding interaction between them. The Hg atom deviates from the $Pt_3$ plane by 2.505 Å. The average Pt−Pt bond length is 2.670 Å, ranging from 2.6680(2) to 2.6775(3) Å, which are slightly longer than those found in **2a** (average 2.643 Å) and **2b** (2.658 Å) and indicate the presence of Pt−Pt single bonds. The three dpppn ligands support the $Hg_2Pt_6$ cluster core in a $D_3$ helical arrangement (Figure 2b). The phosphorus atoms are terminally coordinated to the Pt atoms and are considerably deformed inward with respect to the $Pt_3$ plane, deviations from the plane being 0.413 Å (P1), 0.450 Å (P2), and 0.383 Å (P3). These structural distortions demonstrate that the inner space of the closed cage with dpppn is the minimum necessary to accommodate two mercury atoms in it (Figure 2a). In contrast, the three bridging isocyanide ligands are deformed outward with deviations from the plane of 0.489 Å (C1), 0.312 Å (C2), and 0.548 Å (C3), due presumably to avoiding steric repulsion between the xylyl groups and the phenyl rings of the diphosphine ligands. The dihedral angles between the $Pt_3$ and the $Pt_2C$ planes are 17.8° (C1), 10.8° (C2), and 20.4° (C3). The view along the Hg−Hg axis (Figure 2b) also exhibited the arrangement of three isocyanides in a pseudo-$C_3$ chiral fashion with bending C−N−C structures (average C−N−C = 139.0° (136.5−140.4°)). The three xylyl rings show a fan-shaped structure with the dihedral angles vs the $Pt_3$ triangle ranging between 58.9 and 62.7°.

ORTEP plots of complex **6a** are shown in Figures 3 and 4, and selected bond lengths and angles are listed in Table 3. Complex **6a** has a crystallographic $C_2$ axis passing through the middle points of the C49−C49* and the Hg1−Hg1* bonds and contains a $Pt_3Hg_2Pt_3$ cluster

**Table 2. Selected Bond Lengths (Å) and Angles (deg) for $[Hg_2Pt_6(\mu\text{-XylNC})_6(\mu\text{-dpppn})_3]\cdot C_6H_{14}$ ($8a\cdot C_6H_{14}$)**

| | | | |
|---|---|---|---|
| Hg(1)−Hg(1)* | 2.8424(2) | Hg(1)−Pt(1) | 2.9448(1) |
| Hg(1)−Pt(2) | 2.9541(1) | Hg(1)−Pt(3) | 2.9263(4) |
| Pt(1)−Pt(2) | 2.6680(2) | Pt(1)−Pt(3) | 2.6775(3) |
| Pt(1)−P(1) | 2.253(1) | Pt(1)−C(1) | 2.074(4) |
| Pt(1)−C(3) | 2.064(4) | Pt(2)−Pt(3) | 2.6702(3) |
| Pt(2)−P(2) | 2.260(1) | Pt(2)−C(1) | 2.088(4) |
| Pt(2)−C(2) | 2.181(4) | Pt(3)−P(3) | 2.252(1) |
| Pt(3)−C(2) | 2.088(4) | Pt(3)−C(3) | 2.061(4) |
| N(1)−C(1) | 1.209(6) | N(1)−C(11) | 1.431(6) |
| N(2)−C(2) | 1.188(5) | N(2)−C(21) | 1.386(6) |
| N(3)−C(3) | 1.231(6) | N(3)−C(31) | 1.408(6) |
| Hg(1)*−Hg(1)−Pt(1) | 149.341(6) | Hg(1)*−Hg(1)−Pt(2) | 148.130(6) |
| Hg(1)*−Hg(1)−Pt(3) | 147.629(8) | Pt(1)−Hg(1)−Pt(2) | 53.781(4) |
| Pt(1)−Hg(1)−Pt(3) | 54.263(4) | Pt(2)−Hg(1)−Pt(3) | 54.009(4) |
| Hg(1)−Pt(1)−Pt(2) | 63.288(4) | Hg(1)−Pt(1)−Pt(3) | 62.517(7) |
| Hg(1)−Pt(1)−P(1) | 111.15(3) | Hg(1)−Pt(1)−C(1) | 96.5(1) |
| Hg(1)−Pt(1)−C(3) | 96.1(1) | Pt(2)−Pt(1)−Pt(3) | 59.937(6) |
| Pt(2)−Pt(1)−P(1) | 149.11(3) | Pt(2)−Pt(1)−C(1) | 50.4(1) |
| Pt(2)−Pt(1)−C(3) | 106.9(1) | Pt(3)−Pt(1)−P(1) | 147.67(3) |
| Pt(3)−Pt(1)−C(1) | 108.4(1) | Pt(3)−Pt(1)−C(3) | 49.5(1) |
| P(1)−Pt(1)−C(1) | 103.8(1) | P(1)−Pt(1)−C(3) | 103.9(1) |
| C(1)−Pt(1)−C(3) | 142.9(2) | Hg(1)−Pt(2)−Pt(1) | 62.932(4) |
| Hg(1)−Pt(2)−Pt(3) | 62.464(7) | Hg(1)−Pt(2)−P(2) | 110.52(3) |
| Hg(1)−Pt(2)−C(1) | 95.9(1) | Hg(1)−Pt(2)−C(2) | 91.0(1) |
| Pt(1)−Pt(2)−Pt(3) | 60.208(6) | Pt(1)−Pt(2)−P(2) | 145.82(3) |
| Pt(1)−Pt(2)−C(1) | 49.9(1) | Pt(1)−Pt(2)−C(2) | 109.2(1) |
| Pt(3)−Pt(2)−P(2) | 150.10(3) | Pt(3)−Pt(2)−C(1) | 108.2(1) |
| Pt(3)−Pt(2)−C(2) | 49.7(1) | P(2)−Pt(2)−C(1) | 101.4(1) |
| P(2)−Pt(2)−C(2) | 104.2(1) | C(1)−Pt(2)−C(2) | 149.1(1) |
| Hg(1)−Pt(3)−Pt(1) | 63.221(7) | Hg(1)−Pt(3)−Pt(2) | 63.526(8) |
| Hg(1)−Pt(3)−P(3) | 111.31(3) | Hg(1)−Pt(3)−C(2) | 93.7(1) |
| Hg(1)−Pt(3)−C(3) | 96.7(1) | Pt(1)−Pt(3)−Pt(2) | 59.856(7) |
| Pt(1)−Pt(3)−P(3) | 146.37(3) | Pt(1)−Pt(3)−C(2) | 112.0(1) |
| Pt(1)−Pt(3)−C(3) | 49.6(1) | Pt(2)−Pt(3)−P(3) | 150.92(3) |
| Pt(2)−Pt(3)−C(2) | 52.9(1) | Pt(2)−Pt(3)−C(3) | 106.9(1) |
| P(3)−Pt(3)−C(2) | 101.3(1) | P(3)−Pt(3)−C(3) | 102.1(1) |
| C(2)−Pt(3)−C(3) | 148.8(2) | C(1)−N(1)−C(11) | 140.4(4) |
| C(2)−N(2)−C(21) | 136.5(4) | C(3)−N(3)−C(31) | 140.0(4) |
| Pt(1)−C(1)−Pt(2) | 79.7(2) | Pt(1)−C(1)−N(1) | 142.9(3) |
| Pt(2)−C(1)−N(1) | 133.5(3) | Pt(2)−C(2)−Pt(3) | 77.4(1) |
| Pt(2)−C(2)−N(2) | 135.3(3) | Pt(3)−C(2)−N(2) | 138.7(3) |
| Pt(1)−C(3)−Pt(3) | 80.9(1) | Pt(1)−C(3)−N(3) | 134.3(3) |
| Pt(3)−C(3)−N(3) | 144.5(4) | | |

(23) Braunstein, P.; Rossell, O.; Seco, M.; Torra, I.; Solans, X.; Miravitlles, C. *Organometallics* **1986**, *5*, 1113.

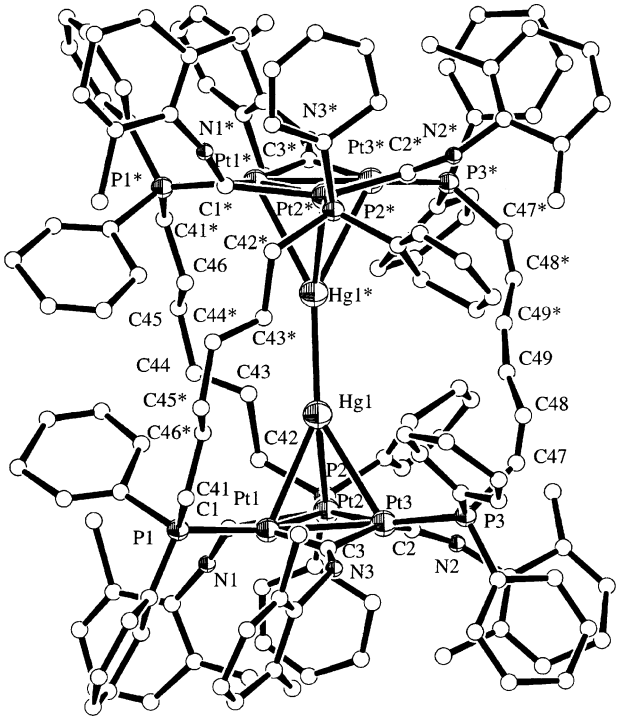


**Figure 3.** ORTEP plot of $[Hg_2Pt_6(\mu\text{-XylNC})_6(dpphx)_3]$ (**6a**).

core supported by three dpphx ligands. Unlike complex **8a**, the two $HgPt_3$ tetrahedrons glide away from each other to lose $C_3$ symmetry, resulting in a declined-antiprismatic structure (parts a and b of Figure 4). A similar structure was observed in the carbonyl-bridged cluster **2b**, but the metal−metal bond distances around the Hg atoms were quite different. The centroids of the $Pt_3$ triangles ($CenPt_3$) and the two Hg atoms are deformed from linearity ($CenPt_3$−Hg1−Hg1* = 169.8°; Figure 4a); however, despite the declined structure, the Hg1−Hg1* bond length of 2.826(2) Å is slightly shorter than is found in **8a**. The separation between the centroids of the $Pt_3$ triangles (7.789 Å) is also slightly shorter than the value in **8a** (7.851 Å), despite the longer methylene chains of dpphx. The average P−P separation of the dpphx ligands is 8.54 Å. The Hg atom lies asymmetrically above the $Pt_3$ triangle by 2.494 Å with nonequivalent Pt−Hg distances: Hg1−Pt1 = 2.937(3) Å, Hg1−Pt2 = 2.858(3) Å, and Hg1−Pt3 = 2.980(3) Å (average 2.925 Å). These structural features suggested that the stronger Hg−Hg interaction, in comparison with **2b**, is intrinsic to the isocyanide-bridged clusters with dpppn and dpphx ligands. The $\{Pt_3(\mu\text{-CNR})_3P_3\}$ units are approximately symmetrical with Pt1−Pt2 = 2.643(4) Å, Pt1−Pt3 = 2.647(3) Å, and Pt2−Pt3 = 2.627(4) Å, and the two $Pt_3$ triangles are nearly parallel with a dihedral angle of 4.1° and are arranged in a staggered form. The extent of inward and outward deformations for the terminal P and the bridging C atoms are rather small compared with those of **8a**; the deviations from the plane are −0.287 Å (P1), 0.026 Å (P2), −0.238 Å (P3), 0.218 Å (C1), 0.498 Å (C2), and 0.280 Å (C3). The dihedral angles between the $Pt_3$ and the $Pt_2C$ planes are 7.0° (C1), 18.2° (C2), and 11.2° (C3). The longer methylene chain with dpphx may release the strains of the planar $Pt_3P_3C_3$ units; in particular, the strain around the Pt2 atom is significantly released. The arrangement of the three isocyanide ligands is largely

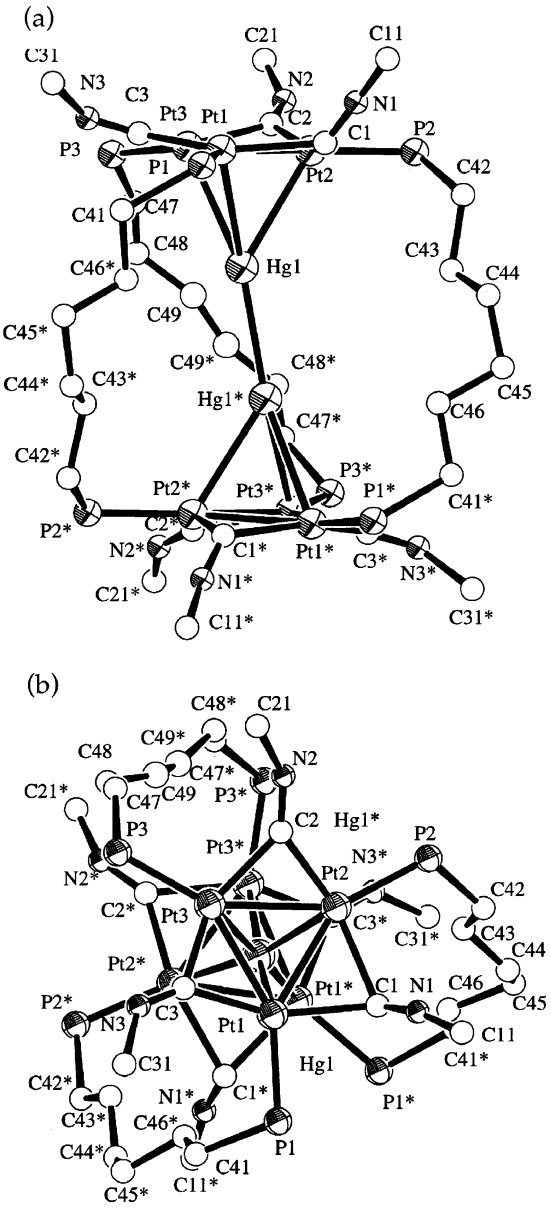


**Figure 4.** ORTEP diagrams for the cluster core of $[Hg_2Pt_6(\mu\text{-XylNC})_6(dpphx)_3]$ (**6a**) viewed (a) vertical to and (b) along the Hg−Hg axis. The phenyl and xylyl rings are omitted for clarity.

distorted from the pseudo-$C_3$ chiral symmetry as observed in **8a**, where two isocyanides show a bent structure with C2−N2−C21 = 147(6)° and C3−N3−N31 = 133(4)° and, in contrast, the other one adopts a relatively linear form with C1−N1−C11 = 167(5)°. The linear bridging isocyanide is not unusual, and the xylyl ring is vertical to the $Pt_3$ plane (98.1°) to reduce the steric repulsion.

**Molecular Orbital Calculations.** To understand the electronic structures of the $Hg_2Pt_6$ clusters with diphosphines (dpppn, dpphx) and, in particular, to elucidate the reasons why the isocyanide-bridged hexaplatinum cage $[Pt_6(\mu\text{-CNR})_6(diphos)_3]$ encapsulated two mercury atoms, in contrast with the fact that the carbonyl-bridged cage $[Pt_6(\mu\text{-CO})_6(diphos)_3]$ incorporated only a mercury atom, molecular orbital calculations were performed with extended Hückel and DFT methods.

EHMO calculations were carried out on $[Hg_2\{Pt_3(\mu\text{-CNH})_3(PH_3)_3\}_2]$ (**I**) as a $D_{3h}$ ideal model for complex **8a**

**Table 3. Selected Bond Lengths (Å) and Angles (deg) for $[Hg_2Pt_6(\mu\text{-XylNC})_6(\mu\text{-dpphx})_3]$ (6a)**

| | | | |
|---|---|---|---|
| Hg(1)−Hg(1)* | 2.826(2) | Hg(1)−Pt(1) | 2.937(3) |
| Hg(1)−Pt(2) | 2.858(3) | Hg(1)−Pt(3) | 2.980(3) |
| Pt(1)−Pt(2) | 2.643(4) | Pt(1)−Pt(3) | 2.647(3) |
| Pt(1)−P(1) | 2.25(2) | Pt(1)−C(1) | 2.18(6) |
| Pt(1)−C(3) | 1.98(5) | Pt(2)−Pt(3) | 2.627(4) |
| Pt(2)−P(2) | 2.22(2) | Pt(2)−C(1) | 2.26(5) |
| Pt(2)−C(2) | 2.03(6) | Pt(3)−P(3) | 2.20(2) |
| Pt(3)−C(2) | 2.11(7) | Pt(3)−C(3) | 1.92(5) |
| N(1)−C(1) | 1.14(7) | N(1)−C(11) | 1.33(7) |
| N(2)−C(2) | 1.22(7) | N(2)−C(21) | 1.43(8) |
| N(3)−C(3) | 1.12(7) | N(3)−C(31) | 1.58(7) |
| Hg(1)*−Hg(1)−Pt(1) | 154.8(1) | Hg(1)*−Hg(1)−Pt(2) | 138.0(1) |
| Hg(1)*−Hg(1)−Pt(3) | 150.5(1) | Pt(1)−Hg(1)−Pt(2) | 54.25(7) |
| Pt(1)−Hg(1)−Pt(3) | 53.14(6) | Pt(2)−Hg(1)−Pt(3) | 53.43(8) |
| Pt(2)−Pt(1)−Hg(1) | 61.36(8) | Pt(2)−Pt(1)−Pt(3) | 59.6(1) |
| Pt(2)−Pt(1)−C(3) | 105(1) | Pt(2)−Pt(1)−P(1) | 145.1(5) |
| Pt(2)−Pt(1)−C(1) | 54(1) | Pt(3)−Pt(1)−Hg(1) | 64.28(8) |
| Pt(3)−Pt(1)−C(3) | 46(1) | Pt(3)−Pt(1)−P(1) | 153.7(5) |
| Pt(3)−Pt(1)−C(1) | 114(1) | P(1)−Pt(1)−Hg(1) | 114.1(3) |
| P(1)−Pt(1)−C(3) | 109(1) | P(1)−Pt(1)−C(1) | 91(1) |
| C(1)−Pt(1)−Hg(1) | 89(1) | C(1)−Pt(1)−C(3) | 155(1) |
| C(3)−Pt(1)−Hg(1) | 91(1) | Pt(3)−Pt(2)−Hg(1) | 65.67(8) |
| Pt(3)−Pt(2)−Pt(1) | 60.29(9) | Pt(3)−Pt(2)−C(1) | 111(1) |
| Pt(3)−Pt(2)−P(2) | 151.0(3) | Pt(3)−Pt(2)−C(2) | 51(2) |
| P(2)−Pt(2)−Hg(1) | 119.9(3) | P(2)−Pt(2)−Pt(1) | 148.7(3) |
| P(2)−Pt(2)−C(1) | 96(1) | P(2)−Pt(2)−C(2) | 100(2) |
| C(1)−Pt(2)−Hg(1) | 89(1) | C(1)−Pt(2)−Pt(1) | 51(1) |
| C(1)−Pt(2)−C(2) | 153(2) | C(2)−Pt(2)−Hg(1) | 99(1) |
| C(2)−Pt(2)−Pt(1) | 110(2) | P(3)−Pt(3)−Hg(1) | 117.0(4) |
| P(3)−Pt(3)−Pt(1) | 149.3(5) | P(3)−Pt(3)−Pt(2) | 149.4(5) |
| P(3)−Pt(3)−C(3) | 102(1) | P(3)−Pt(3)−C(2) | 103(1) |
| C(2)−Pt(3)−Hg(1) | 93(1) | C(2)−Pt(3)−Pt(1) | 107(1) |
| C(2)−Pt(3)−Pt(2) | 49(1) | C(2)−Pt(3)−C(3) | 147(1) |
| C(3)−Pt(3)−Hg(1) | 91(1) | C(3)−Pt(3)−Pt(1) | 48(1) |
| C(3)−Pt(3)−Pt(2) | 107(1) | C(1)−N(1)−C(11) | 167(5) |
| C(2)−N(2)−C(21) | 147(6) | C(3)−N(3)−C(31) | 133(4) |
| Pt(1)−C(1)−Pt(2) | 73(1) | Pt(1)−C(1)−N(1) | 131(4) |
| Pt(2)−C(1)−N(1) | 118(4) | Pt(2)−C(2)−Pt(3) | 78(2) |
| Pt(2)−C(2)−N(2) | 143(5) | Pt(3)−C(2)−N(2) | 137(5) |
| Pt(1)−C(3)−Pt(3) | 85(1) | Pt(1)−C(3)−N(3) | 142(3) |
| Pt(3)−C(3)−N(3) | 132(3) | | |

(Hg−Hg = 2.84 Å, Pt−Hg = 2.68 Å, CenPt$_3$−Hg−Hg = 180°), and the simplified MO interaction diagram with the $[\{Pt_3(\mu\text{-CNH})_3(PH_3)_3\}_2]$ (**Ia**) and the $Hg_2$ (**Ib**) fragments is shown in Figure 5. Since the two $Pt_3$ units are separated at 7.84 Å, there is no through-space interaction between the two triangles and almost no difference was observed between the $D_{3h}$ eclipsed and the $D_{3v}$ staggered models (we chose here the $D_{3h}$ model). The HOMO ($3a_1$) of the triplatinum unit $[Pt_3(\mu\text{-CNH})_3(PH_3)_3]$ (**Ia′**) is composed of an in-phase combination of three $d_{x^2-y^2}$ platinum orbitals, which are known, in general, to be responsible for the Lewis basicity of the $Pt_3$ unit.[2a,c,5a,24] The LUMO ($1a_2$) and the next LUMO ($4a_1$) of **Ia′** are derived from $d_\pi-p_\pi$ and $p_\pi-p_\pi$ bonding interactions of the three Pt atoms and the three bridging isocyanides, respectively. Notably, when the bridging isocyanides are replaced by CO, the energy levels for the lowest unoccupied $1a_2$ and $4a_1$ orbitals were significantly lowered, owing to the $\pi^*$ orbital of CO being lower lying than that of isocyanide. The occupied $3a_1$ and the empty $4a_1$ orbitals of **Ia′** play important roles in constructing the $Hg_2Pt_6$ cluster, as described below.

In the model complex **I**, the occupied $3a_2''$ orbital of the fragment **Ia** repulsively interacts with the $s_{\sigma^*}$ orbital ($1a_2''$) of the $Hg_2$ unit (**Ib**) to generate the bonding ($2a_2''$) and the antibonding ($3a_2''$) molecular orbitals of **I** in a first approximation. The former $2a_2''$ molecular orbital is further mixed with the low-lying d orbitals of the $Pt_3$ units ($1a_2''$ and $2a_2''$ of **Ia**). The latter $3a_2''$ molecular orbital is the HOMO of $[Hg_2\{Pt_3(\mu\text{-CNH})_3(PH_3)_3\}_2]$ (**I**) and is slightly stabilized by in-phase mixing of the $4a_2''$ fragment MO of **Ia**. This in-phase combination of the $4a_2''$ fragment MO increases the nonbonding character of the HOMO of **I** ($3a_2''$) and may result in partial electron migration from the $Hg_2$ atoms to the $Pt_3$ units, whereas the extent of the combination is very small at the EHMO level. The $3a_1'$ and $4a_1'$ fragment MO's of **Ia** potentially interact with the $p_\sigma$ orbital ($2a_1'$) of the $Hg_2$ units, generating the $2a_1'$ and $3a_1'$ MO's of **I**, although the stabilizing effects are very small in the EHMO calculations. The overlap population analysis of the two fragments **Ia** and **Ib** showed that the strongest overlap appeared in the $3a_2''$ MO ($4a_2''$ of **Ia** and $1a_2''$ of **Ib**) and the $2a_1'$ MO ($3a_1'$ of **Ia** and $2a_1'$ of **Ib**); there is no strong overlap in the lower lying fragment orbitals. The $3a_1'$ MO of **I** is considered as the actual LUMO, on the basis of the DFT calculations described below. The slight but appreciable stabilizing effects observed in the $3a_2''$ (HOMO) and $2a_1'$ (next HOMO) orbitals may be responsible for the weak Hg−Pt bonding interaction observed in the structure of **8a**. The bond overlap populations are Hg−Hg = 0.355, Hg−Pt = 0.139, and Pt−Pt = 0.174, indicating the weaker Hg−Pt bonding interaction compared with the Hg−Hg and Pt−Pt bonds. When the Hg−Hg distance increases from 2.84 Å to 3.23 Å, the stabilizing effects by the $4a_2''$ fragment MO (**Ia**) mixing into the HOMO and by the $2a_1'$ fragment MO (**Ib**) mixing into the next HOMO of **I** are remarkably reduced due to the increased HOMO−LUMO energy separation of the $Hg_2$ unit (**Ib**) and the bond overlap populations are reduced to Hg−Hg = 0.132 and Hg−Pt = 0.130.

The single-point DFT calculations for the actual structure of $[Hg_2Pt_6(\mu\text{-XylNC})_6(\mu\text{-dpppn})_3]$ (**8a**) were performed, and the diagrams for the important MO's are shown in Figure 6. The LUMO (MO598) corresponds to the $3a_1'$ orbital of **I** at the EHMO level and is composed of a bonding interaction between the $p_\pi$ orbitals of the $Pt_3$ unit and the $p_\sigma$ orbital of the $Hg_2$

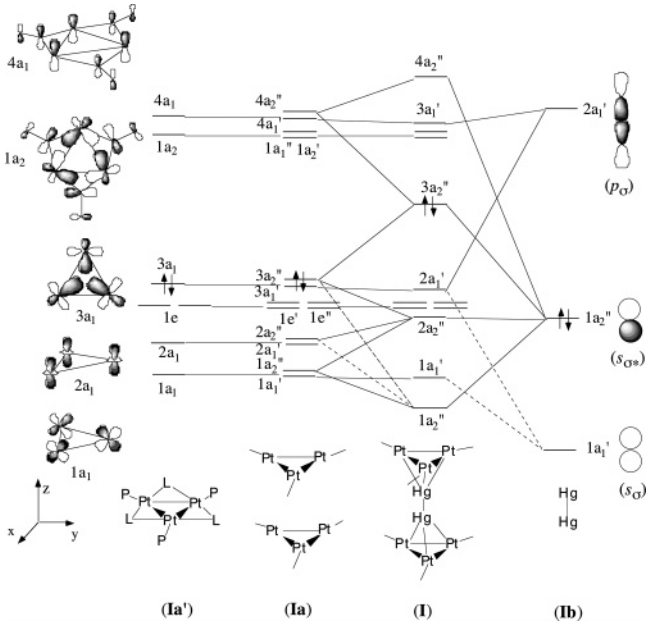


**Figure 5.** MO interaction diagram for the $D_{3h}$ model complex $[Hg_2\{Pt_3(\mu\text{-CNH})_3(PH_3)_3\}_2]$ (**I**) from the $\{Pt_3(\mu\text{-CNH})_3(PH_3)_3\}_2$ (**Ia**) and the $Hg_2$ (**Ib**) fragments on the basis of EHMO calculations.

(24) Underwood, D. J.; Hoffmann, R.; Tatsumi, K.; Nakamura, A.; Yamamoto, Y. *J. Am. Chem. Soc.* **1985**, *107*, 5968.

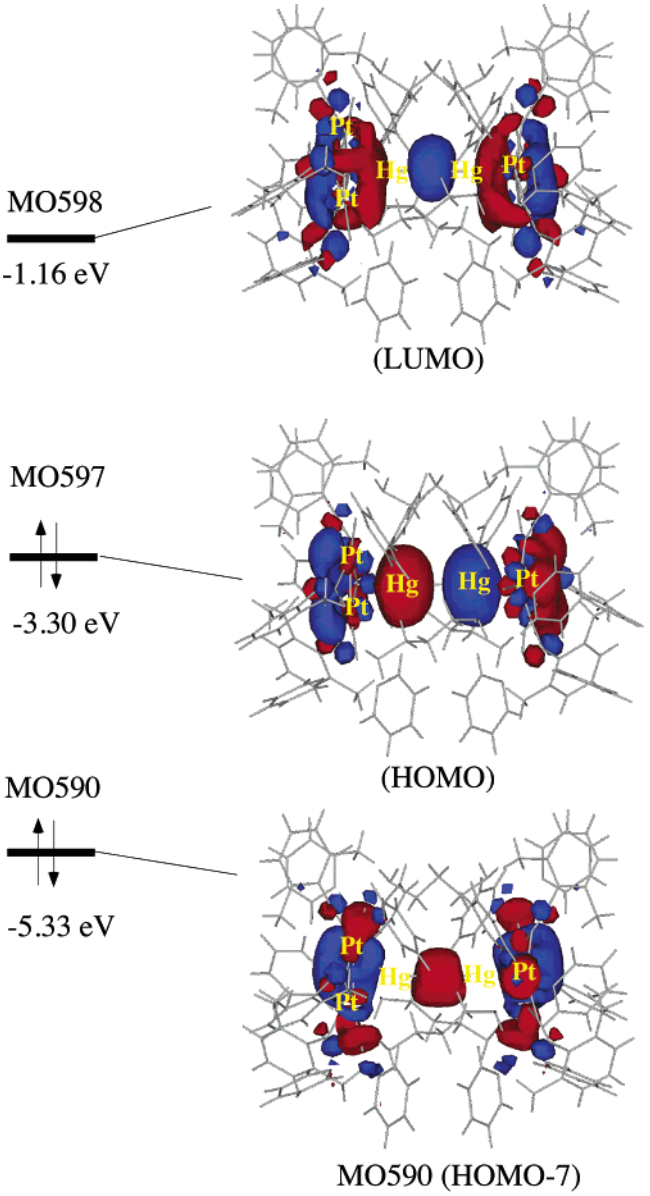


**Figure 6.** MO diagrams for $[Hg_2Pt_6(\mu\text{-XylNC})_6(dpppn)_3]$ (**8a**) on the basis of DFT single-point calculations.

atoms. The HOMO (MO597) definitely shows a nonbonding character between the Hg and $Pt_3$ atoms by in-phase combination of $p_\pi$ orbitals of the $Pt_3$ units into the antibonding interaction between the platinum d orbitals and the $s_{\sigma^*}$ orbital of the $Hg_2$ atoms, as observed in the EHMO calculations. The stabilizing combination of the platinum $p_\pi$ orbitals in the HOMO results in a sufficient HOMO−LUMO energy gap of 2.14 eV. In the HOMO (MO597) and LUMO (MO598), the contributions from the $\pi^*$ orbitals of the bridging isocyanides are smaller than are expected in the EHMO level, because of their outward-bending structures. The HOMO-7 (MO 590), corresponding to the $2a_1'$ orbital of **I**, is significantly stabilized by the bonding interaction of the $Hg_2$ $p_\sigma$ orbital with the platinum d orbitals of the $Pt_3$ units. These results are essentially in accord with those from the EHMO calculations and strongly suggest that the Hg−Hg distance should be determined to gain the best overlap between the LUMO of the $\{Pt_3\}_2$ units and the HOMO of the dimercury atoms and vice versa.[25]

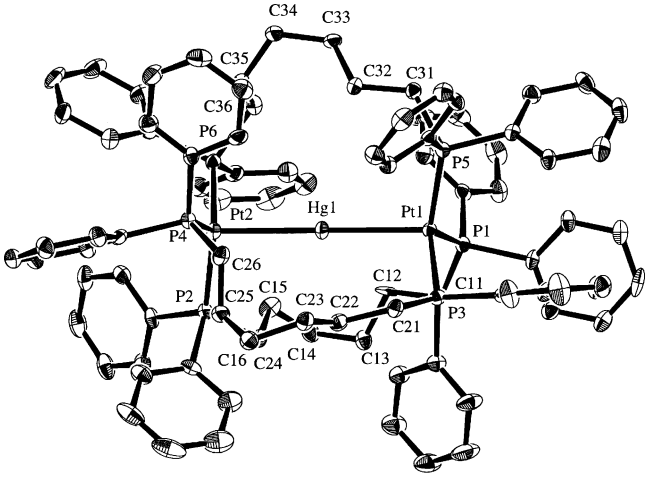


**Figure 7.** ORTEP plot of $[HgPt_2(\mu\text{-dpphx})_3]$ (**11**).

**Table 4. Selected Bond Lengths (Å) and Angles (deg) for $[HgPt_2(\mu\text{-dpphx})_3]\cdot 3.5C_6H_6$ ($11\cdot 3.5C_6H_6$)**

| | | | |
|---|---|---|---|
| Hg(1)−Pt(1) | 2.7908(4) | Hg(1)−Pt(2) | 2.7952(4) |
| Pt(1)−P(1) | 2.279(2) | Pt(1)−P(3) | 2.281(2) |
| Pt(1)−P(5) | 2.273(2) | Pt(2)−P(2) | 2.287(2) |
| Pt(2)−P(4) | 2.288(2) | Pt(2)−P(6) | 2.291(2) |
| Pt(1)−Hg(1)−Pt(2) | 179.58(2) | Hg(1)−Pt(1)−P(1) | 102.76(4) |
| Hg(1)−Pt(1)−P(3) | 101.13(4) | Hg(1)−Pt(1)−P(5) | 101.72(4) |
| P(1)−Pt(1)−P(3) | 114.64(6) | P(1)−Pt(1)−P(5) | 116.37(6) |
| P(3)−Pt(1)−P(5) | 116.64(5) | Hg(1)−Pt(2)−P(2) | 99.14(4) |
| Hg(1)−Pt(2)−P(4) | 97.81(4) | Hg(1)−Pt(2)−P(6) | 95.84(4) |
| P(2)−Pt(2)−P(4) | 117.30(6) | P(2)−Pt(2)−P(6) | 117.49(6) |
| P(4)−Pt(2)−P(6) | 120.07(6) | | |

When the bridging isocyanides are replaced by carbonyl ligands, the EHMO calculations suggest that the HOMO−LUMO gap of the $Hg_2Pt_6$ cluster becomes remarkably small, due to the low-lying CO $\pi^*$ orbitals. The stronger in-phase mixing of the $p_\pi$ orbitals of the $Pt_3$ units into the HOMO may promote an electron transfer from the $Hg_2$ unit to the $Pt_3$ fragments, which might be subject to concomitant structural changes or decomposition. When the Hg−Hg distance increases, the energy of the filled $s_{\sigma^*}$ orbital for the $Hg_2$ unit will be reduced, and consequently, the HOMO of $[Hg_2\{Pt_3(\mu\text{-}CO)_3(PH_3)_3\}_2]$ will be stabilized to result in an appropriate HOMO−LUMO gap. Otherwise, the two $\{Pt_3(\mu\text{-}CO)_3(PH_3)_3\}$ units are likely to sandwich a single Hg atom, where the lower lying filled Hg s orbital can decrease the energy for the HOMO of $[Hg\{Pt_3(\mu\text{-}CO)_3(PH_3)_3\}_2]$. The number of mercury atoms incorporated between the two $Pt_3$ units may depend on the energy levels for the lowest unoccupied molecular orbitals of the $\{Pt_3(\mu\text{-}L)_3P_3\}$ triplatinum unit (L = RNC, CO).

**Trinuclear Complex of $[HgPt_2(\mu\text{-dpphx})_3]$ (11).** The structure of **11** was determined by X-ray crystallography; an ORTEP diagram is given in Figure 7, and selected bond distances and angles are listed in Table 4. Two three-coordinate platinum atoms are held together by three dpphx ligands to form a pseudo-$D_3$ symmetrical cage, at the center of which a single mercury atom is trapped. This is the first example of a

(25) The single-point DFT calculations for the structure of **6a**, consisting of the declined $Pt_3Hg_2Pt_3$ core, provided a set of frontier orbitals essentially identical with those shown in **8a**. The HOMO is slightly destabillized by mixing of the p orbitals of the $Hg_2$ unit, and the donor/acceptor interactions (from Hg s to Pt p and from Pt d to Hg p) occur predominantly at the Pt2 atom, which has the shortest Pt−Hg distance of 2.858(3) Å.

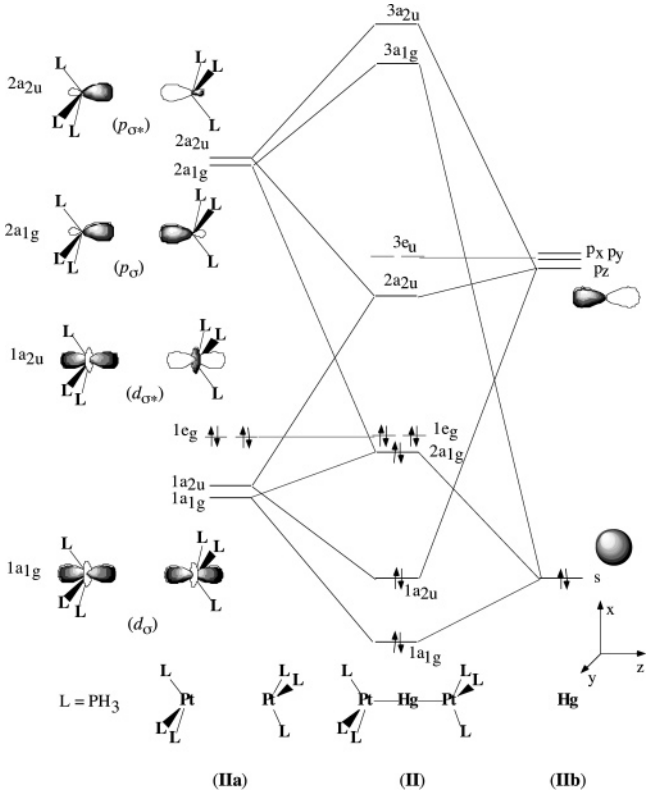


**Figure 8.** MO interaction diagram for a model complex [Hg{Pt(PH$_3$)$_3$}$_2$] (**II**) from the {Pt(PH$_3$)$_3$}$_2$ (**IIa**) and the Hg (**IIb**) fragments on the basis of EHMO calculations.

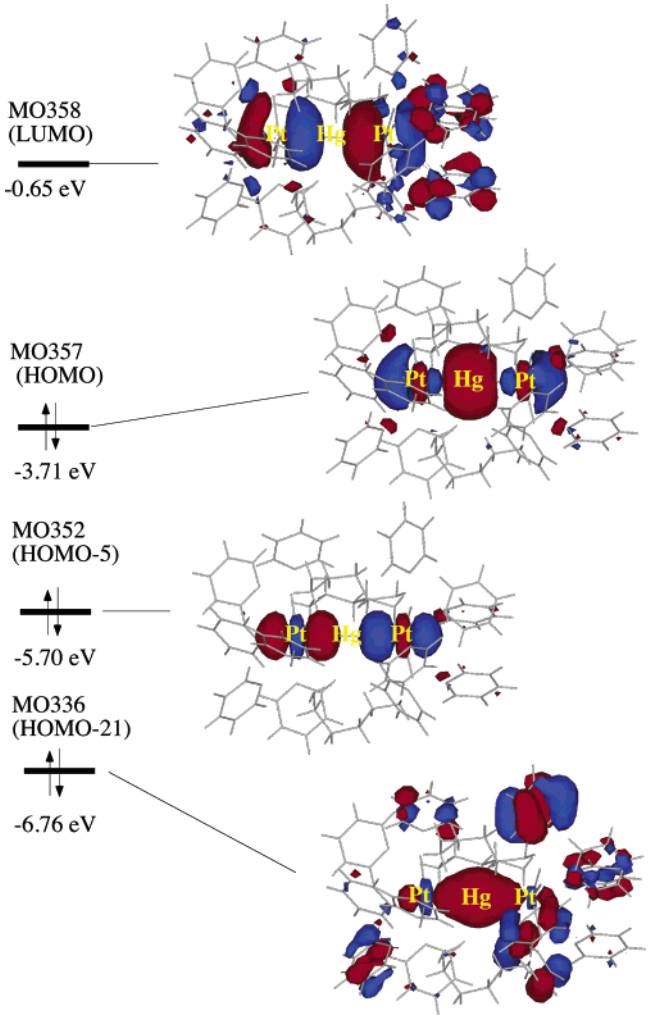


**Figure 9.** MO diagrams for [HgPt$_2$($\mu$-dpphx)$_3$] (**8a**) on the basis of DFT single-point calculations.

trinuclear complex containing a linear Pt(0)−Hg(0)−Pt(0) metallic core. The Pt atoms are deformed from their respective trigonal P$_3$ planes toward the Hg atom by 0.469 Å (Pt1) and 0.302 Å (Pt2). The two P$_3$ triangles around the Pt atoms are parallel, with a dihedral angle of 1.6°, and are arranged in a staggered form. The Pt−Hg bond lengths are nearly equal (Pt1−Hg1 = 2.7908(4) Å and Pt2−Hg1 = 2.7952(4) Å (average 2.7930 Å)), and the three metal atoms are ordered in an almost linear arrangement (Pt1−Hg1−Pt2 = 179.58(2)°). The Hg−Pt distances are longer than the Pt(I)−Hg(0)−Pt(I) covalent bonds observed in [HgPt$_2$(diphos)$_2$(XylNC)$_2$](PF$_6$)$_2$ (diphos = *cis*-1,2-bis(diphenylphosphino)ethene (2.615(1) Å), 1,3-bis(diphenylphosphino)propane (average 2.640 Å), 1,2-bis(di-*tert*-butylphosphino)ethane (2.6409(9) Å))[12a] but almost comparable to the sum of the covalent radii (Pt = 1.30 Å, Hg = 1.49 Å), indicating the presence of a considerable attractive interaction between the Pt and the Hg atoms. Similar structures with d$^{10}$−d$^{10}$s$^2$−d$^{10}$ metal systems were reported in [Au$_2$Hg(P$_2$phen)$_3$](PF$_6$)$_2$ (P$_2$phen = 2,9-bis(diphenylphosphino)-1,10-phenanthroline, average Au−Hg = 2.783 Å),[26a] [M$_2$Tl(P$_2$phen)$_3$]$^+$ (M = Pt, average Pt−Tl = 2.7913 Å; M = Pd, Pd−Tl = 2.7914(6) Å),[26b] [M$_2$Tl(P$_2$bpy)$_3$]$^+$ (P$_2$bpy = 6,6′-bis(diphenylphosphino)-2,2′-bipyridine; M = Pt, Pt−Tl = 2.7953(2) Å; M = Pd, Pd−Tl = 2.7678(6) Å),[26b] and [Pd$_2$Pb(P$_2$phen)$_3$]$^{3+}$ (average Pd−Pb = 2.6999 Å).[26c] The two Pt atoms are separated at 5.586 Å, and the average distance between the two phosphorus atoms of dpphx ligands is 6.73 Å, which is significantly shorter than is found in the Hg$_2$Pt$_6$ cluster **6a** (average 8.54 Å). There is no interaction between the Hg atom and the methylene chains of the diphosphine ligands.

Since the structure of **11** demonstrated the relatively short Pt−Hg bond distances, MO calculations were carried out with EHMO and DFT methods to elucidate the electronic structures concerning the Pt−Hg interaction. The interaction diagram for the $D_{3d}$ model complex [(H$_3$P)$_3$PtHgPt(PH$_3$)$_3$] (**II**) was analyzed with the fragments of [(H$_3$P)$_3$Pt···Pt(PH$_3$)$_3$] (**IIa**) and Hg$^0$ (**IIb**) (Figure 8). Two conspicuous interactions between the two fragments are observed on the basis of the overlap population analysis. One interaction is derived from the 1a$_{1g}$ (d$_\sigma$) and 2a$_{1g}$ (p$_\sigma$) fragment MO's and the s orbital of the Hg atom to generate the 1a$_{1g}$, 2a$_{1g}$, and 3a$_{1g}$ molecular orbitals by bonding, nonbonding, and antibonding interactions, respectively. The first two are occupied, and the last one is unoccupied. The second interaction is derived from the 1a$_{2u}$ (d$_{\sigma^*}$) and 2a$_{2u}$ (p$_{\sigma^*}$) fragment MO's and the empty $p_z$ orbital of the Hg atom to result in 1a$_{2u}$, 2a$_{2u}$, and 3a$_{2u}$ molecular orbitals with the first one occupied and the other two unoccupied. From these interactions, the strength of the Pt−Hg bond should be dependent on the extent of mixing of the 2a$_{1g}$ fragment MO (**IIa**) into the 2a$_{1g}$ MO with in-phase interaction, which may increase the nonbonding character and stabilize the 2a$_{1g}$ MO of **II**. The bond overlap

(26) (a) Catalano, V. J.; Malwitz, M. A.; Noll, B. C. *Chem. Commun.* **2001**, 581. (b) Catalano, V. J.; Bennett, B. L.; Yson, R. L.; Noll, B. C. *J. Am. Chem. Soc.* **2000**, *122*, 10056. (c) Catalano, V. J.; Bennett, B. L.; Noll, B. C. *Chem. Commun.* **2000**, 1413.

population between the Pt and Hg atoms is 0.277, nearly corresponding to a Pt−Hg single bond. The single-point DFT calculations for the actual structure of $[HgPt_2(\mu\text{-dpphx})_3]$ (**11**) were carried out to afford results comparable to those from the EHMO calculations (Figure 9). MO358 (LUMO), MO357 (HOMO), MO352 (HOMO-5), and MO336 (HOMO-21) are essentially corresponding to the $2a_{2u}$, $2a_{1g}$, $1a_{2u}$, and $1a_{1g}$ orbitals, respectively, at the EHMO level (Figure 8). The MO358 (LUMO) is high lying, with a bonding interaction between the $p_{\sigma^*}$ orbitals of the $Pt_2$ atoms and the p orbital of the Hg atom. MO352 (HOMO-5) and MO336 (HOMO-21) are considerably stabilized by bonding combinations of the $Pt_2$ $d_{\sigma^*}$ and $d_\sigma$ orbitals with the Hg p and s orbitals, respectively, which are responsible for the linear Pt−Hg−Pt bonding structure. In the HOMO (MO357), partial nonbonding character between the Pt and Hg atoms arises from the in-phase mixing of the $p_\sigma$ orbitals of the Pt atoms into the repulsive interaction between the $Pt_2$ $d_\sigma$ orbitals and the Hg s orbital, which should be responsible for the relatively strong Hg−Pt bonds observed in the structure of **11**.

## Conclusion

In the present study, the cage-type $Hg_2Pt_6$ mixed-metal clusters $[Hg_2Pt_6(\mu\text{-RNC})_6(\text{diphos})_3]$ (diphos = dpphx, R = Xyl (**6a**); diphos = dpppn, R = Xyl (**8a**), Mes (**8b**)) were synthesized from reduction of $[PtCl_2(cod)]$ using bulky aromatic isocyanides and diphosphines having long methylene chains and were characterized by X-ray crystallography to demonstrate that two $Pt_3$ triangular units of $\{Pt_3(\mu\text{-RNC})_3\}$ are held together by three diphosphine ligands to constitute a large-size closed cage in which two zerovalent mercury atoms are incorporated. The molecular orbital calculations suggested that the donating and the accepting characters by the HOMO and LUMO of the $Pt_3$ units are important to stabilize the $Hg_2Pt_6$ structure and are influenced by the Hg−Hg distance as well as the bridging ligands. When *t*-BuNC was used instead of the bulky aromatic isocyanides, the linear $HgPt_2$ trinuclear complex $[HgPt_2(\mu\text{-dpphx})_3]$ (**11**) was isolated as the first characterized example of a Pt(0)−Hg(0)−Pt(0) trinuclear complex.

**Acknowledgment.** This work was partly supported by a Grant-in-Aid for Scientific Research from Ministry of Education, Culture, Sports, Science, and Technology of Japan.

**Supporting Information Available:** Tabulation of X-ray crystallographic data, including experimental details, atomic parameters, and bond distances and angles of complexes **6a, 8a**, and **11**. This material is available free of charge via the Internet at http://pubs.acs.org.

OM049251X